

An energy-conserving discontinuous multiscale finite element method for the wave equation in heterogeneous media

Eric T. Chung* Yalchin Efendiev† Richard L. Gibson, Jr.‡

February 5, 2011

Abstract

Seismic data are routinely used to infer *in situ* properties of earth materials on many scales, ranging from global studies to investigations of surficial geological formations. While inversion and imaging algorithms utilizing these data have improved steadily, there are remaining challenges that make detailed measurements of the properties of some geologic materials very difficult. For example, the determination of the concentration and orientation of fracture systems is prohibitively expensive to simulate on the fine grid and, thus, some type of coarse-grid simulations are needed. In this paper, we describe a new multiscale finite element algorithm for simulating seismic wave propagation in heterogeneous media. This method solves the wave equation on a coarse grid using multiscale basis functions and a global coupling mechanism to relate information between fine and coarse grids. Using a mixed formulation of the wave equation and staggered discontinuous basis functions, the proposed multiscale methods have the following properties.

- The total wave energy is conserved.
- Mass matrix is diagonal on a coarse grid and explicit energy-preserving time discretization does not require solving a linear system at each time step.
- Multiscale basis functions can accurately capture the subgrid variations of the solution and the time stepping is performed on a coarse grid.

*Department of Mathematics, The Chinese University of Hong Kong, Hong Kong. (tschung@math.cuhk.edu.hk)

†Department of Mathematics, Texas A & M University, College Station, TX 77843. (efendiev@math.tamu.edu)

‡Department of Geology & Geophysics, Texas A & M University, College Station, TX 77843. (gibson@tamu.edu)

We discuss various subgrid capturing mechanism and present some preliminary numerical results.

1 Introduction

Seismic data provide important constraints on *in situ* earth properties on many scales, ranging from global studies to investigations of the properties of shallow soils and surficial geologic formations comprising the first several meters of the earth. A broad variety of methods have been developed to analyze the data to provide images of earth structure, including tomography algorithms that provide 3-D images of structure from wavefields propagating through, and possibly scattered by, the geological features of interest [43, 31, 45, 40, 4, 33, 36, 15]. Other solutions emphasize the analysis of reflected waves, especially from artificial sources of seismic waves, and such measurements provide some of the most important information for applications such as hydrocarbon exploration [2, 14, 26, 3]. Recent research has also been extending the application of such methods to apply them to seismic waves generated by natural sources to image the structure of Earth's crust and mantle [5, 42, 28].

However, significant challenges remain when the goal is to relate seismic measurements to detailed variations in rock properties, e.g., fractured media. For example, CO₂ sequestration provides a compelling approach for mitigating the global warming effects of greenhouse gases [1]. Sequestration in geologic formations such as known hydrocarbon reservoirs provides one of the most mature and effective technologies for reduction of greenhouse gas levels [41, 1, 25, 6]. Nonetheless, challenges in the implementation of sequestration efforts remain, as long term storage of CO₂ faces potential difficulties associated with potential movement of CO₂ through fractures, processes that may be accelerated because of the low density and viscosity of CO₂ [19]. Geochemical reactions over long time scales also complicate the process [24, 29, 18, 12]. Seismic reflection data have significant potential for monitoring the movement of CO₂, since the low bulk modulus and density lead to strong contrasts in elastic properties of rock, thereby facilitating the detection of leaks. However, heterogeneities have a critical influence on subsurface fluid flow because of the dramatic contrast in permeability between fractures and the surrounding rock, and because the fracture network thereby controls the overall flow patterns. An important goal is therefore not only to use seismic data to detect CO₂, but also to infer fine-scale features of the earth materials.

Given the practical importance of incorporating the influence of fine-scale heterogeneities into seismic modeling and inversion algorithms, there are therefore strong incentives to develop new, more accurate, efficient numerical modeling schemes to provide more reliable results. Current practice in modeling seismic wave propagation in complex, 3-D media typically relies on finite difference solutions to the wave equation using regular, Cartesian grids. These algorithms in principle provide exact results, but there are important limitations. First, the discretization is typically on the order of 10 to 20 m in each coordinate direction, with results restricted to relatively low

frequencies (e.g., 30 Hz) [35, 34]. When the targets of interest are subtle features such as fracture distributions, this discretization may be too coarse to accurately describe them. Recent studies show that there are inherent sources of error in regular grid finite difference algorithms because they do not accurately model the geometry of interfaces [34]. Furthermore, models are forced to rely on upscaling procedures to estimate elastic properties on the coarse grid, and there is no guarantee that this will provide accurate and reliable results [23]. In the presence of complex heterogeneities, the accuracy of upscaling methods deteriorate. In fact, complex fracture networks can introduce important non-local effects that can not be approximated via simple upscaling methods [30, 22]. To capture the effects of these features, more complex subgrid models need to be introduced that can take into account important non-local features.

In this paper, we present a new class of energy-preserving discontinuous multiscale finite element methods for modeling wave propagation in heterogeneous media. The multiscale finite element methods we propose offer a flexible approach that has not yet been applied to seismic wave propagation in detail. The main idea of these approaches is to represent the effects of the small scales on the large ones by constructing multiscale basis functions. This allows performing the time discretization on a coarse grid. We note that there are several multiscale methods (e.g., [39, 37, 38, 17]) that are proposed in the literature for solving wave equations. To our best knowledge, [39] is the first paper where the multiscale method is employed to solve wave equation. Our work shares similarities with [39, 37, 38], though it has some important differences. In particular, we employ a different coarse-scale discretization that allows having diagonal mass matrices that are easy to invert. We would like to use the proposed methods when the coarse grid is not too coarse and is capable of resolving the initial condition. For this reason, it is important to have a diagonal mass matrix that will help to speed-up the computations substantially. Another difference between the proposed method and the methods in [39, 37, 38] is that they are based on different multiscale coupling frameworks though these frameworks share similarities.

One of the main aspects of the proposed methods is the construction of multiscale basis functions that can capture the effects of the small scales accurately. In our previous work [22], we have developed several subgrid models where the basis functions accomplish this goal. In particular, we have used both local and global information within mixed and Galerkin discretization of wave equations in [22]. In general, this approach solves the relevant equations on a coarse grid using pre-computed basis functions that can recover the fine-scale features of the solution such as those that would be generated by fractures. However, the mass matrices in this formulation are not local and may require expensive inversions within explicit schemes. Recently, there are newly developed optimal discontinuous Galerkin methods [10, 9] that give both explicit and energy conserving numerical schemes. Following the framework in [10, 9], our proposed approaches avoid the inversion of global mass matrices by allowing multiscale basis functions to have discontinuities. In designing multiscale finite element methods, we consider mixed formulations of the wave equation. With

appropriate temporal discretizations, this allows the design of numerical schemes that conserve energy, which is important in simulations of wave propagation. Numerical results are presented.

Our proposed approach can be seen as a multiscale FDTD method and the co-volume method [7] for wave simulations. All these methods are known to be explicit and energy conserving, and are hence very efficient for the numerical approximation of waves.

2 Coarse-scale multiscale finite element discretization

In this section, we will describe a coarse-scale formulation of the wave equation. We will use a formulation that provides energy conservation and results in an explicit scheme. Local multiscale basis functions will be employed to demonstrate the main concept of these new multiscale coupling techniques. We will discuss advanced subgrid capturing mechanisms and how to improve our methods by representing local features more accurately.

To describe the coarse-scale formulation, we let Ω be a bounded domain in R^d ($d = 2, 3$) and $T > 0$. We will consider the acoustic wave equations in mixed form

$$\rho \frac{\partial u}{\partial t} - \nabla \cdot v = f, \quad (x, t) \in \Omega \times [0, T], \quad (1)$$

$$A \frac{\partial v}{\partial t} - \nabla u = 0, \quad (x, t) \in \Omega \times [0, T]. \quad (2)$$

The extension to elastic wave equations is under investigation.

In the above system (1)-(2), the scalar function $u(x, t)$, representing pressure for example, and the vector field $v(x, t)$, representing particle velocity for example, are the unknowns to be approximated. The function f is a source term. The coefficient $\rho(x)$ satisfies $\rho(x) \geq \rho_0 > 0$ and the $d \times d$ symmetric matrix A satisfies $q^T A q \geq a_0 |q|^2$, with $a_0 > 0$, for all $q \in R^d$ and for all $x \in \Omega$. We supplement the system (1)-(2) with the homogeneous Neumann boundary conditions $v \cdot n = 0$ on $\partial\Omega$ and initial conditions $u(x, 0) = u_0(x)$ and $v(x, 0) = v_0(x)$ for $x \in \Omega$.

One important physical property described by the system (1)-(2) is the following conservation of energy: if $f = 0$, then

$$\frac{d}{dt} \int_{\Omega} \frac{1}{2} (\rho u^2 + v^T A v) dx = 0, \quad \frac{d}{dt} \int_{\Omega'} \frac{1}{2} (\rho u^2 + v^T A v) dx = \int_{\partial\Omega'} u (v \cdot n) d\sigma \quad (3)$$

for any subdomain $\Omega' \subset \Omega$. We would like to preserve this relation in our numerical simulations. We will use the main concepts developed in [10] to achieve the energy conservation and diagonal mass matrices. We would like to point out that there have been many developments within finite element methods for the wave equation in mixed formulation and for the elastic wave equation [13, 21, 32, 11]. In particular,

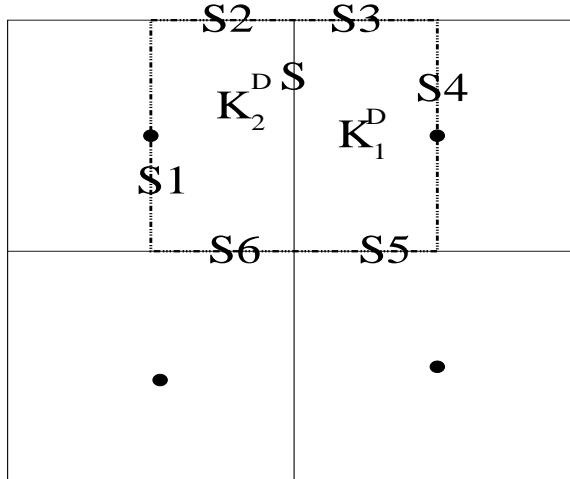


Figure 1: Illustration of rectangular elements for mixed multiscale basis functions.

the mixed finite element methods developed in [21, 11] result in block diagonal mass matrices. In this paper we follow the framework presented in [10].

In [22], a general mixed finite element formulation of wave equations is presented that can use multiple local information in constructing multiscale basis functions. However, in this formulation, the mass matrix is global, and it is computationally expensive to invert this matrix. Our goal is to develop a mixed multiscale finite element approach where the mass matrix is block diagonal and easy to invert by employing discontinuous basis functions for v . We present this approach for rectangular domains. These methods can be extended to handle general unstructured grids.

We will follow the conceptual discretization framework proposed in [10]. Similar finite elements have been proposed for flow in porous media in [27]. For these approaches, the mass matrix is block diagonal and basis functions are discontinuous, allowing more flexibility. To describe the basis functions, we first consider rectangular elements. In Figure 1, four coarse blocks are plotted. Each piecewise constant basis function η for u is supported in each rectangle K . Next, we will define basis functions for v .

Basis functions for v are defined for each edge of a coarse block. The key idea of our approach is that, for each edge of a coarse block, we will only define a basis for the normal component of v , where the normal direction is the one that is perpendicular to the edge. We show this construction for one of the edges S as it is depicted in Figure 1. The support of this basis function ψ_S is restricted to $K_1^D \cup K_2^D$, i.e., only half of each rectangular element having the edge S . To construct multiscale basis functions, we first find λ_S such that it solves the following equations in K_1^D and K_2^D :

$$\nabla \cdot \lambda_S = 0, \quad \lambda_S = A^{-1} \nabla \phi_S. \quad (4)$$

In each K_1^D and K_2^D , the solution is subject to the following boundary conditions:

$$\lambda_S \cdot n = 0 \quad \text{on } S_2, S_3, S_5, S_6. \quad (5)$$

For the edge S , we have

$$\lambda_S \cdot n = 1 \quad \text{on } S, \quad (6)$$

where S is the length of the edge S . Because we would like to have divergence free λ_S , the unit flow needs to be distributed on S_1 and S_4 . One can use various distributions depending on the spatial variations in heterogeneous material properties (see discussions later). Here, for simplicity we use

$$\begin{aligned} \lambda_S \cdot n &= 1 \quad \text{on } S_1 \\ \lambda_S \cdot n &= 1 \quad \text{on } S_4. \end{aligned} \quad (7)$$

Then the basis function for the edge S is defined as $\psi_S = \lambda_S \cdot n$ where n is the unit normal vector for the edge S . The above construction is to demonstrate the basis function for the edge S and this process is repeated for each coarse-grid block edge. These basis functions are used to represent v , $v = \sum_S v_S \psi_S$, where v_S are coarse-scale values of the solution on the edge S .

We remark that for the case with constant coefficient, that is when A is a scalar multiple of the identity matrix, the basis function $\psi_S = 1$ everywhere on $K_1^D \cup K_2^D$. Thus our method reduces to the standard FDTD method for wave propagation [44]. In this sense, the method developed in this paper can be seen as a multiscale FDTD method for wave simulations.

We denote basis functions for representing u by η and basis functions for representing v by ψ . Notice that at each point in the domain except those discontinuous points of ψ , we can write $\psi = (\psi_S, 0)^T$ or $\psi = (0, \psi_S)^T$ for some edge S . We denote the coarse space spanned by basis functions η by U_h and the coarse space spanned by velocity basis functions by V_h . The coarse-scale problem is defined as follows. Find $u_h \in U_h$ and $v_h \in V_h$ such that for all $z \in U_h$ and $q \in V_h$ we have

$$\int_{\Omega} \rho \frac{\partial u_h}{\partial t} z \, dx + B_h(v_h, z) = F_h(z), \quad (8)$$

$$\int_{\Omega} A \frac{\partial v_h}{\partial t} \cdot q \, dx - B_h^*(u_h, q) = 0, \quad (9)$$

where F_h , B_h and B_h^* are defined by

$$F_h(z) = \int_{\Omega} f z \, dx \quad (10)$$

$$B_h(v_h, z) = - \sum_K \int_{\partial K} (v_h \cdot n) z \, d\sigma, \quad (11)$$

$$B_h^*(u_h, q) = \sum_{K_S} \int_{\partial K_S} u_h (q \cdot n) \, d\sigma, \quad (12)$$

where in (11) K denotes the support of a basis function in U_h while in (12) K_S denotes the support of a basis function in V_h . By the construction of the spaces U_h and V_h , we will show that the operator B_h^* is the adjoint of B_h (see also [10, 9]) in the following lemma. This is the key step for energy conservation.

Lemma 1 For all $z \in U_h$ and $q \in V_h$ we have

$$B_h(q, z) = B_h^*(z, q).$$

Proof. By the definition of B_h ,

$$\begin{aligned} B_h(q, z) &= - \sum_K \int_{\partial K} (q \cdot n) z \, d\sigma \\ &= \int_{\Omega} q \cdot \nabla z \, dx - \sum_K \int_{\partial K} (q \cdot n) z \, d\sigma, \end{aligned}$$

where the last equality follows from the fact that z is a piecewise constant function, and the gradient operator is defined element-wise. Applying element-wise Green's identity (see also [10]), we obtain

$$B_h(q, z) = - \int_{\Omega} z \nabla \cdot q \, dx + \sum_{K_S} \int_{\partial K_S} z (q \cdot n) \, d\sigma.$$

We recall that q is taken as a divergence-free vector, see (4). Hence

$$B_h(q, z) = \sum_{K_S} \int_{\partial K_S} z (q \cdot n) \, d\sigma = B_h^*(z, q).$$

□

Writing the system (8)-(9) in matrix form, we get

$$M_1 \frac{dU}{dt} + BV = F, \quad (13)$$

$$M_2 \frac{dV}{dt} - B^T U = 0, \quad (14)$$

where U is the vector of coefficients in the expansion $u_h = \sum_i u_i \eta_i$ and V is the vector of coefficients in the expansion $v_h = \sum_S v_S \psi_S$. The vector F is defined as $F_i = F_h(\eta_i)$ and the matrix B is defined by $B_{ij} = B(\psi_i, \eta_j)$. The mass matrices M_1 and M_2 are defined by

$$(M_1)_{ij} = \int_{\Omega} \rho \eta_i \eta_j \, dx, \quad (M_2)_{ij} = \int_{\Omega} \psi_i^T A \psi_j \, dx.$$

Since the basis functions η_i in U_h and ψ_j in V_h have disjoint supports, M_1 and M_2 are diagonal matrices.

The time discretization for our scheme will use a leap-frog scheme which conserves energy (see e.g. [8]). The resulting discretization has the form: given $(U^n, V^{n+\frac{1}{2}})$, find $(U^{n+1}, V^{n+\frac{3}{2}})$ by solving

$$M_1 U^{n+1} = M_1 U^n - \Delta t B V^{n+\frac{1}{2}} + \Delta t F^{n+\frac{1}{2}} \quad (15)$$

$$M_2 V^{n+\frac{3}{2}} = M_2 V^{n+\frac{1}{2}} + \Delta t B^T U^{n+1}, \quad (16)$$

where U^n represents the function $u_h(x, t_n)$ and $V^{n+\frac{1}{2}}$ represents the function $v_h(x, t_{n+\frac{1}{2}})$. Note that since M_1 and M_2 are diagonal matrices, the system (15)-(16) can be trivially inverted.

2.1 Discussion on subgrid capturing

The approach discussed above employs the constant boundary conditions for multiscale basis functions defined in (5), (6), and (7). It is known that these boundary conditions result in resonance errors [20, 16] and, thus, give large subgrid errors. The utilization of local solutions in larger domains, oversampling, improves subgrid capturing [20]. Oversampling methods use the solutions of the local problems in larger domains to impose boundary conditions. In some cases, these regions will be taken as a whole domain (as in [16]). Once these local solutions are defined, they are used in turn to impose boundary conditions for multiscale basis functions. Several alternatives for implementing oversampling have been proposed (e.g., see [16] for a review). We can also study the extensions of these basis functions when we need to span several vector fields. In particular, we will use v_i 's to impose boundary conditions for the basis functions on the interior edges (faces). The main goal is to span v_1, \dots, v_N with the constructed multiscale basis functions. This extension is needed for achieving better subgrid accuracy.

One can show that the proposed approach can recover the homogenized solution when there is a scale separation, e.g., when $A = A(y)$, $y = x/\epsilon$, is a periodic function with respect to y . In particular, using first-order corrector expansion of the local solution for the basis function, $\psi_i = A^{-1}(I + \epsilon \nabla_y N) \nabla \eta_i^0 + \dots$, where N is the solution of the cell problem, $\nabla_y \cdot A^{-1}(I + \nabla_y N) = 0$, η_i^0 is the homogenized component of η_i we can show that the mass matrix M_2 is approximately the same as the mass matrix that corresponds to the wave problem with homogenized coefficients. The rigorous proof of this fact is more difficult. Similar results can be shown for M_1 . This also indicates that one can use local solutions in smaller representative volumes ([16]), e.g., in a periodic cell for periodic heterogeneities, to compute M_2 when there is a scale separation.

In this paper, our main goal is to discuss multiscale coupling and a new multiscale basis functions that are discontinuous. In a subsequent paper, we will study advanced subgrid capturing mechanisms that employ oversampling or limited global information. The proposed methods can be extended to unstructured coarse grids.

3 Numerical results

In this section, we present some preliminary numerical results. We only consider multiscale basis functions with constant boundary conditions (see (5), (6), and (7)), but we will present results for several models of heterogeneous distributions of material properties. Our main goal is to show that the proposed methods provide a robust framework for coupling discontinuous multiscale basis functions. As we mentioned, some attractive features of the proposed methods are (1) energy conservation and (2) local mass matrix on a coarse grid. The first set of test results demonstrates the accuracy of the solutions for arbitrary, smoothly varying initial conditions, and the second set of solutions shows that our scheme correctly handles models of that

localized, point sources that are typically applied in seismic reflection experiments.

3.1 Examples with smoothly varying initial conditions

In our first set of numerical simulations, we take $\rho = 1$ and compare results for various distributions of isotropic, scalar coefficients $A = A(x)\delta_{ij}$. In these examples, the fine grid is 400×400 , the coarse grid is 20×20 , and the domain size is 1×1 . Zero Neumann boundary conditions are imposed on external boundaries. Initial velocity v is taken to be zero and the initial pressure field u is taken to be

$$u(x_1, x_2) = \cos(\pi x_1) + \cos(\pi x_2).$$

We note that initial conditions need to be resolved on the coarse grid for multiscale methods, as is the case for this simulation; otherwise extra basis functions are needed to represent additional fine-scale features due to initial conditions or source terms. We present simulation results at $t = 0.3$.

In the first numerical example, we take

$$A^{-1}(x_1, x_2) = 3 + \sin^2(80\pi x_1) + \sin^2(80\pi x_2). \quad (17)$$

In Figure 2, we depict the total wave energy for the fine-scale solution (red) and coarse-scale solution (blue). The coarse-scale solution energy is almost the same as that for the fine-scale solution. In Figure 3, we depict both fine- and coarse-scale solutions for u and the x_1 and x_2 components of v at $t = 0.3$. The fine-scale solutions are shown on the top row, while the corresponding coarse-scale solutions are presented on the bottom row. Though there are some discrepancies, the coarse-scale solution captures the main features of the fine-scale solution accurately. Moreover, we do not observe any spurious features in the coarse-scale solutions. Denoting the relative errors in u and the x_1 and x_2 components of v as E_u , E_{v_1} , and E_{v_2} , respectively, we find the following values at $t = 0.3$: $E_u = 0.01$, $E_{v_1} = 0.046$, and $E_{v_2} = 0.046$. All errors are computed using the L_2 norm.

In the second numerical example, A^{-1} is taken a realization of a random field with exponential covariance function

$$\exp\left(-\frac{|x_1 - x_2|}{L_1} - \frac{|y_1 - y_2|}{L_2}\right), \quad (18)$$

where the correlation lengths are $L_1 = 1.0$ and $L_2 = 0.05$. We use standard Karhunen-Loeve expansion to generate a realization of the random field. We take the variance to be $\sigma^2 = 0.2$. Larger variations introduce bigger errors and may require better subgrid capturing mechanisms to obtain accurate approximation of the solution. This is currently under investigation. A^{-1} is plotted in Figure 4 (left). In the right portion of Figure 4, we show the total wave energy for fine-scale solution (designated by red color) and coarse-scale solution (designated by blue color). As for the previous results, the coarse-scale solution predicts the energy accurately. Figure 5 compares the fine-

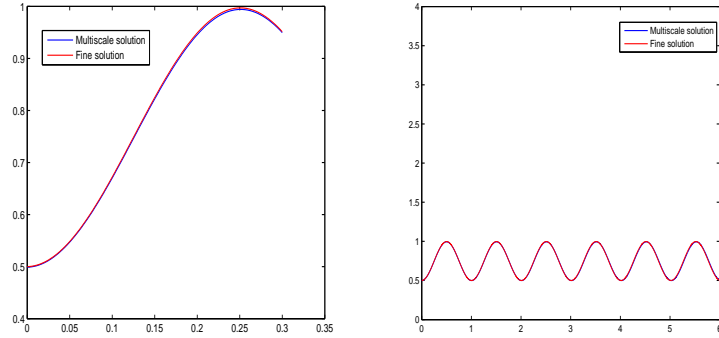


Figure 2: Energy as a function of time for coarse- and fine-scale solutions for shorter (left) and longer (right) time intervals. Periodic case.

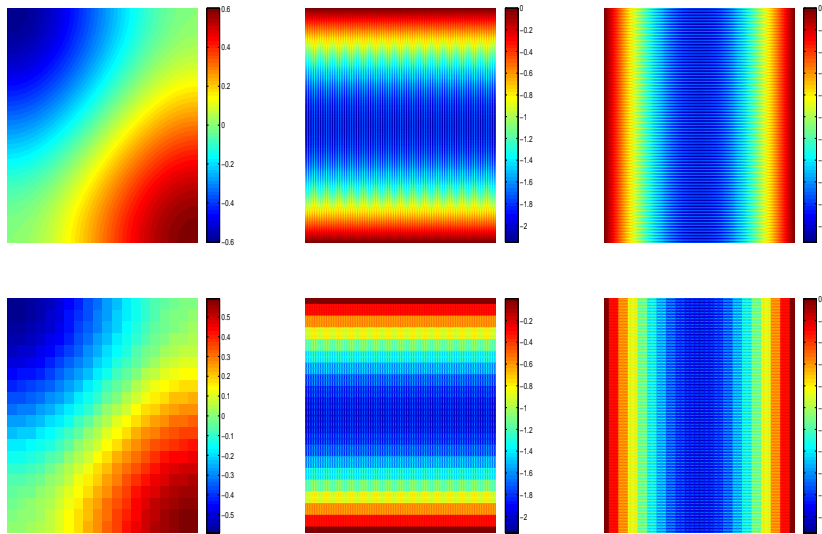


Figure 3: Comparison of the solution at time $t = 0.3$. Top-left: fine-scale solution. Top-middle: fine-scale x_1 component of velocity. Top-right: fine-scale x_2 component of velocity. Bottom-left: coarse-scale solution. Bottom-middle: coarse-scale x_1 -velocity. Bottom-right: coarse-scale x_2 -velocity. Periodic case.

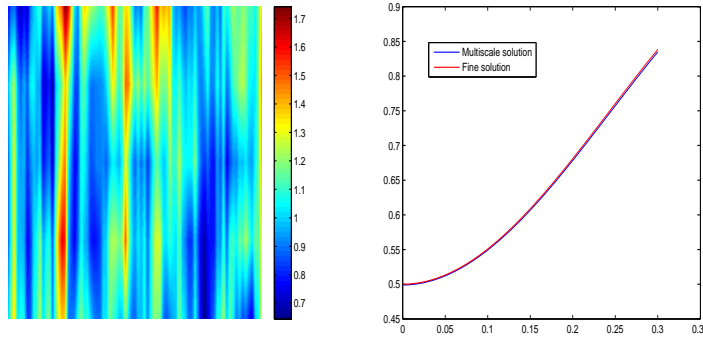


Figure 4: Left: Coefficients A (see 18). Right: Energy as a function of time for coarse- and fine-scale solutions. Random case with $L_1 = 1.0$ and $L_2 = 0.05$.

and coarse-scale solutions u and the two components of v at $t = 0.3$. Fine-scale solutions are depicted on the top row, while corresponding coarse-scale solutions are depicted on the bottom row. The coarse-scale solution captures the main features of the fine-scale solution and the relative errors at $t = 0.3$ are: $E_u = 0.011$, $E_{v_1} = 0.109$, and $E_{v_2} = 0.046$.

In the next numerical example, A^{-1} is again taken as a realization of a random field with exponential covariance function in (18), but the correlation lengths are set to $L_1 = 0.4$ and $L_2 = 0.05$. We again take the variance to be $\sigma^2 = 0.2$. A^{-1} is plotted in Figure 6 (left figure). On the right figure of Figure 6, we depict the total wave energy for fine-scale solution (designated by red color) and coarse-scale solution (designated by blue color). We see that the coarse-scale solution can very accurately approximate the fine-scale solution in terms of total energy. In Figure 7, we depict fine-scale solution u and components of v as well as coarse-scale solution u and component of v at $t = 0.1$ and $t = 0.3$. Fine-scale solutions are depicted on the top row, while corresponding coarse-scale solutions are depicted on the bottom row. Again, we observe that the coarse-scale solution captures the main features of the fine-scale solution. We find the following errors at $t = 0.3$: $E_u = 0.01$, $E_{v_1} = 0.089$, and $E_{v_2} = 0.046$.

3.2 Examples with Gaussian source

Seismic reflection experiments record wavefields generated by localized sources applied to a small volume within the earth or a small area on the surface of the earth. In this next set of examples, we implement such a source to simulate the propagation of body waves that are typically utilized to estimate the properties of earth materials. As in the previous simulations, we take $\rho = 1$. In all of these examples, the fine grid is 2000×2000 , the coarse grid is 200×200 , and the domain size is 1×1 . Zero Neumann boundary conditions are imposed on external boundaries to suppress artificial reflections. Initial velocity v is taken to be zero and the initial pressure field

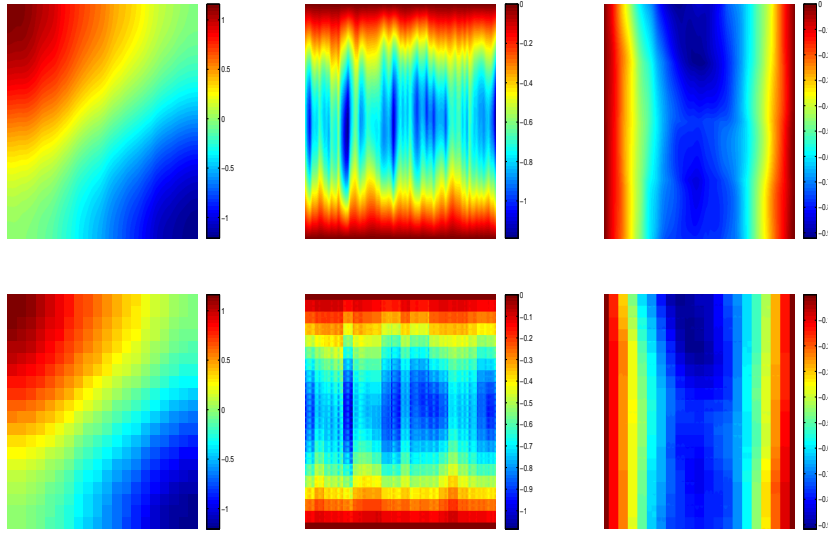


Figure 5: Comparison of the solution at time $t = 0.3$. Top-left: fine-scale solution. Top-middle: fine-scale x_1 component of velocity. Top-right: fine-scale x_2 component of velocity. Bottom-left: coarse-scale solution. Bottom-middle: coarse-scale x_1 velocity component. Bottom-right: coarse-scale x_2 velocity component. Random case with $L_1 = 1.0$ and $L_2 = 0.05$ (Fig. 4).

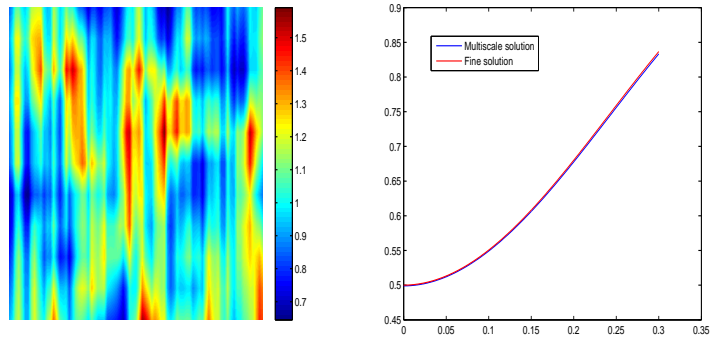


Figure 6: Left: Coefficients (see 18). Right: Energy as a function of time for coarse- and fine-scale solutions. Random case with $L_1 = 0.4$ and $L_2 = 0.05$.

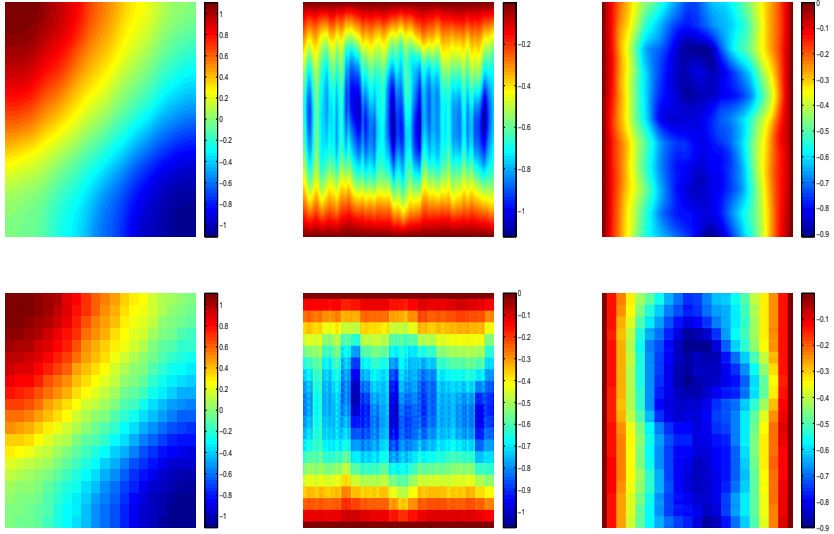


Figure 7: Comparison of the solution at time $t = 0.3$. Top-left: fine-scale solution. Top-middle: fine-scale x_1 component of velocity. Top-right: fine-scale x_2 component of velocity. Bottom-left: coarse-scale solution. Bottom-middle: coarse-scale x_1 velocity component. Bottom-right: coarse-scale x_2 velocity component. Random case with $L_1 = 0.4$ and $L_2 = 0.05$ (Fig. 6).

u is taken to be

$$u(x_1, x_2) = e^{-50\sqrt{(x_1-0.5)^2+(x_2-0.5)^2}}.$$

We take

$$A^{-1}(x_1, x_2) = 3 + \sin^2(800\pi x_1) + \sin^2(800\pi x_2). \quad (19)$$

The initial condition for u and the energy behavior are shown in Figure 8. Numerical results are shown in Figure 9. In Figure 10, we also present the numerical solution obtained with a coarse grid without using the multiscale basis. In the latter, we only solve the problem on a coarse grid and do not perform downscaling with multiscale basis functions. The wave clearly travels with an incorrect velocity. Moreover, the relative errors are $E_u = 0.0916$, $E_{v_1} = 0.106$, and $E_{v_2} = 0.106$.

4 Conclusions

In this paper, we propose a mixed multiscale finite element method that uses discontinuous basis functions. The proposed method can accurately solve wave propagation on a coarse grid. Our methods can be efficient for seismic wave propagation problems where the equations need to be solved many times, and one can re-use multiscale basis functions. Moreover, subgrid information in the multiscale basis functions provides access to fine-scale features of the solution. The proposed methods avoid mass

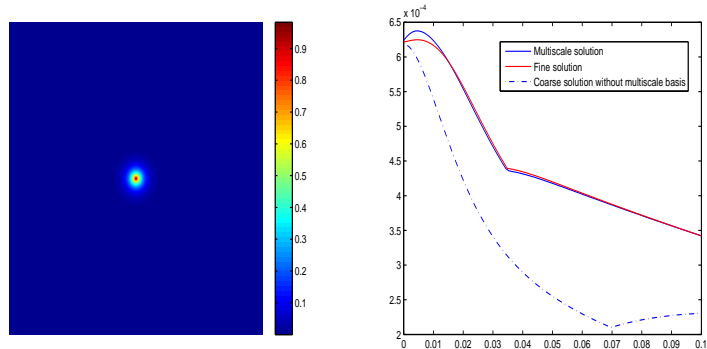


Figure 8: Left: Initial condition for u . Right: Energy as a function of time for coarse-scale solution with multiscale basis functions, fine-scale and coarse-scale solution without using downscaling with multiscale basis functions.

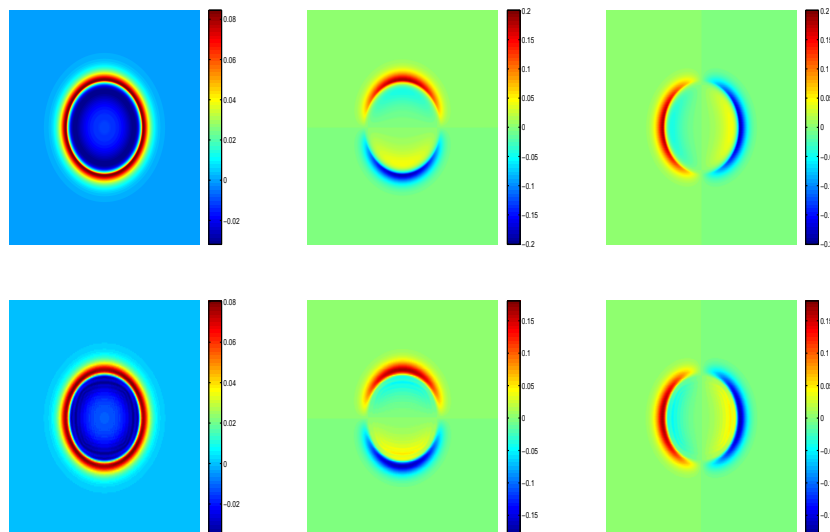


Figure 9: Comparison of the solution at time $t = 0.1$. Top-left: fine-scale solution. Top-middle: fine-scale x_1 component of velocity. Top-right: fine-scale x_2 component of velocity. Bottom-left: coarse-scale solution. Bottom-middle: coarse-scale x_1 velocity component. Bottom-right: coarse-scale x_2 velocity component.

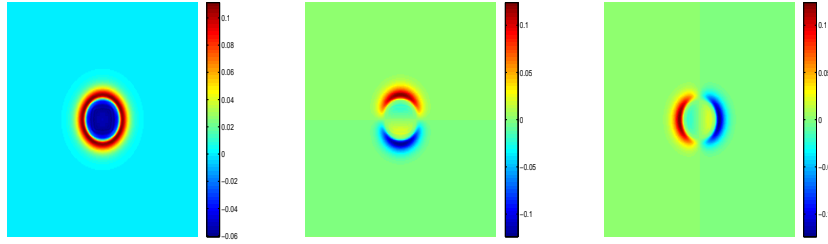


Figure 10: Comparison of the solution at time $t = 0.1$. Left: coarse-scale solution. Middle: coarse-scale x_1 velocity component. Right: coarse-scale x_2 velocity component.

matrix inversion as was demonstrated in the paper. Using leap-frog time discretization, one can achieve energy conservation. In the paper, we also discuss the use of various subgrid capturing mechanisms to improve the accuracy of these multiscale methods by modifying boundary conditions of the basis functions. Numerical results are presented.

5 Acknowledgments

The work of YE is partially supported by Award Number KUS-C1-016-04, made by King Abdullah University of Science and Technology (KAUST). YE's work is partially supported by NSF and DOE. RLG is partially supported by Award Number KUS-C1-016-04, made by King Abdullah University of Science and Technology (KAUST), and by the U.S. Dept. of Energy under grant number Grant No. DE-FG03-00ER15034.

References

- [1] S. Bachu. CO₂ storage in geological media: Role, means, status and barriers to deployment. *Progress in Energy and Combustion Science*, 34(2):254 – 273, 2008.
- [2] G. Beylkin. Imaging of discontinuities in the inverse scattering problem by inversion of a causal generalized Radon transform. *J. Math. Phys.*, 26:99–108, 1985.
- [3] N. Bleistein, J. Cohen, and J. Stockwell, Jr. *Mathematics of multidimensional seismic imaging, migration, and inversion*. Springer-Verlag, New York, 2001.
- [4] L. Boschi, T. W. Becker, G. Soldati, and A. M. Dziewonski. On the relevance of Born theory in global seismic tomography. *Geophysical Research Letters*, 33:L06302, 2006.

- [5] M. G. Bostock and S. Rondenay. Migration of scattered teleseismic body waves. *Geophysical Journal International*, 137(3):732–746, 1999.
- [6] A. Chadwick, R. Arts, O. Eiken, P. Williamson, and G. Williams. Geophysical monitoring of the CO₂ plume at Sleipner, North Sea. *Advances in the Geological Storage of Carbon Dioxide*, pages 303–314, 2006.
- [7] E. T. Chung, Q. Du, and J. Zou. Convergence analysis on a finite volume method for maxwell’s equations in non-homogeneous media. *SIAM J. Numer. Anal.*, 41:37–63, 2003.
- [8] E. T. Chung and B. Engquist. Convergence analysis of fully discrete finite volume methods for maxwell’s equations in nonhomogeneous media. *SIAM J. Numer. Anal.*, 43:303–317, 2005.
- [9] E. T. Chung and B. Engquist. Optimal discontinuous galerkin methods for wave propagation. *SIAM J. Numer. Anal.*, 44:2131–2158, 2006.
- [10] E. T. Chung and B. Engquist. Optimal discontinuous galerkin methods for the acoustic wave equation in higher dimensions. *SIAM Journal on Numerical Analysis*, 47(5):3820–3848, 2009.
- [11] G. Cohen and S. Fauqueux. Mixed spectral finite elements for the linear elasticity system in unbounded domains. *SIAM J. Sci. Comput.*, 26(3):864–884 (electronic), 2005.
- [12] I. Czernichowski-Lauriol, C. Rochelle, I. Gaus, M. Azaroual, J. Pearce, and P. Durst. Geochemical interactions between CO₂, pore-waters and reservoir rocks. *Advances in the Geological Storage of Carbon Dioxide*, pages 157–174, 2006.
- [13] J. D. De Basabe and M. K. Sen. New developments in the finite-element method for seismic modeling. *The Leading Edge*, 28(5):562–567, 2009.
- [14] M. de Hoop and N. Bleistein. Generalized Radon transform inversions for reflectivity in anisotropic elastic media. *Inverse Problems*, 13:669–690, 1997.
- [15] M. Delost, J. Virieux, and S. Operto. First-arrival travelttime tomography using second generation wavelets. *Geophysical Prospecting*, 56(4):505–526, 2008.
- [16] Y. Efendiev and T. Y. Hou. *Multiscale finite element methods*, volume 4 of *Surveys and Tutorials in the Applied Mathematical Sciences*. Springer, New York, 2009. Theory and applications.
- [17] B. Engquist, H. Holst, and O. Runborg. Multi-scale methods for wave propagation in heterogeneous media. *Commun. Math. Sci.*, 9(1):33–56, 2011.

- [18] T. K. Flaathen, S. R. Gislason, E. H. Oelkers, and Á. E. Sveinbjörnsdóttir. Chemical evolution of the Mt. Hekla, Iceland, groundwaters: A natural analogue for CO₂ sequestration in basaltic rocks. *Applied Geochemistry*, 24(3):463 – 474, 2009.
- [19] M. A. Hesse and A. W. Woods. Buoyant dispersal of CO₂ during geological storage. *Geophys. Res. Lett.*, 37, 01 2010.
- [20] T. Hou and X. Wu. A multiscale finite element method for elliptic problems in composite materials and porous media. *J. Comp. Physics*, 134:169–189, 1997.
- [21] E. W. Jenkins, B. Rivière, and M. F. Wheeler. A priori error estimates for mixed finite element approximations of the acoustic wave equation. *SIAM J. Numer. Anal.*, 40(5):1698–1715 (electronic), 2002.
- [22] L. Jiang, Y. Efendiev, and V. Ginting. Global multiscale methods for acoustic wave equations with continuum scales. Submitted, 2009.
- [23] O. S. Krüger, E. H. Saenger, S. J. Oates, and S. A. Shapiro. A numerical study on reflection coefficients of fractured media. *Geophysics*, 72(4):D61–D67, 2007.
- [24] A. Kumar, A. Datta-Gupta, R. Shekhar, and R. L. Gibson. Modeling time lapse seismic monitoring of CO₂ sequestration in hydrocarbon reservoirs including compositional and geochemical effects. *Petroleum Science & Technology*, 26(7/8):887 – 911, 2008.
- [25] K. S. Lackner. CLIMATE CHANGE: A Guide to CO₂ Sequestration. *Science*, 300(5626):1677–1678, 2003.
- [26] G. Lambaré, S. Operto, P. Podvin, and P. Thierry. 3D ray + Born migration/inversion—part 1: Theory. *Geophysics*, 68(4):1348–1356, 2003.
- [27] I. D. Mishev and Q.-Y. Chen. A mixed finite volume method for elliptic problems. *Numer. Methods Partial Differential Equations*, 23(5):1122–1138, 2007.
- [28] R. L. Nowack, W.-P. Chen, U. Kruse, and S. Dasgupta. Imaging offsets in the Moho: Synthetic tests using Gaussian beams with teleseismic waves. *Pure and Applied Geophysics*, 16(10):1921–1936, 2007.
- [29] E. H. Oelkers, S. R. Gislason, and J. Matter. Mineral Carbonation of CO₂. *ELEMENTS*, 4(5):333–337, 2008.
- [30] H. Owhadi and L. Zhang. Numerical homogenization of the acoustic wave equations with a continuum of scales. *Comput. Methods Appl. Mech. Engrg.*, 198(3-4):397–406, 2008.
- [31] R. G. Pratt and M. H. Worthington. The application of diffraction tomography to cross-hole seismic data. *Geophysics*, 53(10):1284–1294, 1988.

- [32] B. Rivière, S. Shaw, M. F. Wheeler, and J. R. Whiteman. Discontinuous Galerkin finite element methods for linear elasticity and quasistatic linear viscoelasticity. *Numer. Math.*, 95(2):347–376, 2003.
- [33] A. Sieminski, Q. Liu, J. Trampert, and J. Tromp. Finite-frequency sensitivity of body waves to anisotropy based upon adjoint methods. *Geophysical Journal International*, 171(1):368–389, 2007.
- [34] W. Symes, I. S. Terentyev, and T. Vdovina. Getting it right without knowing the answer: Quality control in a large seismic modeling project. *SEG Technical Program Expanded Abstracts*, 28(1):2602–2606, 2009.
- [35] P. Thore, I. Tarrass, R. L. Gibson, V. Lisitsa, G. Reshetova, and V. Tcheverda. Accurate generation of seismograms on fractured reservoirs. *International Petroleum Technology Conference, 2009, Doha, Qatar*, 2009.
- [36] Y. Tian, S. H. Hung, G. Nolet, R. Montelli, and F. A. Dahlen. Dynamic ray tracing and traveltimes corrections for global seismic tomography. *Journal of Computational Physics*, 226(1):672–687, 2007.
- [37] T. Vdovina and S. Minkoff. An a priori error analysis of operator upscaling for the acoustic wave equation. *International Journal of Numerical Analysis and Modeling*, 5:543–569, 2008.
- [38] T. Vdovina, S. Minkoff, and S. Griffith. A two-scale solution algorithm for the elastic wave equation. *SIAM J. Scientific Computing*, 31:3356–3386, 2009.
- [39] T. Vdovina, S. Minkoff, and O. Korostyshevskaya. Operator upscaling for the acoustic wave equation. *SIAM Journal on Multiscale Modeling and Simulation*, 4:1305–1338, 2005.
- [40] T. Watanabe, S. Shimizu, E. Asakawa, and T. Matsuoka. Differential waveform tomography for time-lapse crosswell seismic data with application to gas hydrate production monitoring. *SEG Technical Program Expanded Abstracts*, 23(1):2323–2326, 2004.
- [41] D. White, G. Burrowes, T. Davis, Z. Hajnal, K. Hirsche, I. Hutcheon, E. Majer, B. Rostron, and S. Whittaker. Greenhouse gas sequestration in abandoned oil reservoirs: the International Energy Agency Weyburn pilot project. *GSA Today*, 14(7):4–1, July 2004.
- [42] G. Wittlinger, J. Vergne, P. Tapponnier, V. Farra, G. Poupinet, M. Jiang, H. Su, G. Herquel, and A. Paul. Teleseismic imaging of subducting lithosphere and Moho offsets beneath western Tibet. *Earth and Planetary Science Letters*, 221(1-4):117 – 130, 2004.
- [43] M. J. Woodward. Wave-equation tomography. *Geophysics*, 57(1):15–26, 1992.

- [44] K. S. Yee. Numerical solution of initial boundary value problems involving maxwells equations in isotropic media. *IEEE Trans. Antennas Propagat.*, 14:302–307, 1966.
- [45] J. Zhang and M. N. Toksöz. Nonlinear refraction travelttime tomography. *Geophysics*, 63:1726–1737, 1998.